International Journal of Nanomedicine

Dovepress
open access to scientific and medical research

Open Access Full Text Article

ORIGINAL RESEARCH

Injectable Chitosan-Based Thermosensitive Hydrogel/Nanoparticle-Loaded System for Local Delivery of Vancomycin in the Treatment of Osteomyelitis

This article was published in the following Dove Press journal:
International Journal of Nanomedicine

Jin Tao[1]
Yang Zhang[2]
Ao Shen[3]
Yunxu Yang[1]
Lu Diao[4]
Luye Wang[1]
Danwei Cai[4]
Ying Hu[1,4]

[1]School of Pharmaceutical Sciences, Zhejiang Pharmaceutical College, Ningbo, Zhejiang, People's Republic of China; [2]Department of Medicine, Zhejiang Academy of Traditional Chinese Medicine, Hangzhou, Zhejiang, People's Republic of China; [3]School of Chemistry and Molecular Biosciences, The University of Queensland, Brisbane, Queensland 4072, Australia; [4]School of Pharmaceutical Sciences, Wenzhou Medical University, Wenzhou, Zhejiang, People's Republic of China

Purpose: Osteomyelitis, particularly chronic osteomyelitis, remains a major challenge for orthopedic surgeons. The traditional treatment for osteomyelitis, which involves antibiotics and debridement, does not provide a complete solution for infection and bone repair. Antibiotics such as vancomycin (VCM) are commonly used to treat osteomyelitis in clinical settings. VCM use is limited by a lack of effective delivery methods that provide sustained, high doses to entirely fill irregular bone tissue to treat infections.

Methods: We engineered a chitosan (CS)-based thermosensitive hydrogel to produce a VCM-nanoparticle (NPs)/Gel local drug delivery system. The VCM-NPs were formed with quaternary ammonium chitosan and carboxylated chitosan nanoparticles (VCM-NPs) by positive and negative charge adsorption to enhance the encapsulation efficiency and drug loading of VCM, with the aim of simultaneously preventing infection and repairing broken bones. This hydrogel was evaluated in a rabbit osteomyelitis model.

Results: The VCM-NPs had high encapsulation efficiency and drug loading, with values of 60.1±2.1% and 24.1±0.84%, respectively. When embedded in CS-Gel, the VCM-NPs maintained their particle size and morphology, and the injectability and thermosensitivity of the hydrogel, which were evaluated by injectability test and rheological measurement, were retained. The VCM-NPs/Gel exhibited sustained release of VCM over 26 days. In vitro tests revealed that the VCM-NPs/Gel promoted osteoblast proliferation and activity against *Staphylococcus aureus*. In vivo, VCM-NPs/Gel (with 10 mg vancomycin per rabbit) was used to treat rabbits with osteomyelitis. The VCM-NPs/Gel showed excellent anti-infection properties and accelerating bone repair under osteomyelitis conditions.

Conclusion: The reported multifunctional NPs hydrogel system for local antibiotic delivery (VCM-NPs/Gel) showed bone regeneration promotion and anti-infection properties, demonstrating significant potential as a scaffold for effective treatment of osteomyelitis.

Keywords: vancomycin, chitosan, nanoparticles, injectable hydrogel, osteomyelitis

Correspondence: Ying Hu
Zhejiang Pharmaceutical College, No. 888, East Section, Yinxian Main Road, The Zone of Higher Education, Ningbo, Zhejiang 315100, People's Republic of China
Tel +86 574 8822 2707
Fax +86 574 8822 3023
Email pharmhawk@126.com

Introduction

Osteomyelitis is an inflammatory bone disease that is caused by an infecting microorganism and leads to progressive bone destruction and loss.[1] Osteomyelitis can be caused by various pathogens, such as Gram-positive pathogens, Gram-negative pathogens, and *Mycobacterium tuberculosis*. However, it is primarily caused by Gram-positive *staphylococci*, which account for ~75% of the cases.[2,3]

Infection increases the patient's recovery time and can cause other morbidities, adding to the financial burden on the patient and the healthcare system.

Osteomyelitis can be classified into three subforms; acute, sub-acute, and chronic. Acute and sub-acute osteomyelitis occur in children and elderly people as a result of a microbe being present in the blood.[2,4] Chronic osteomyelitis commonly presents with open fractures, diabetes, and other diseases and is becoming more widespread. Chronic osteomyelitis can induce bone defects, osteonecrosis, and lead to a high recurrence of secondary infection.[5,6] Therefore, treating chronic osteomyelitis is often challenging as both the infection and subsequent bone repair must be addressed.

Antibiotic treatments using drugs such as levofloxacin[7] and vancomycin (VCM)[8] are the traditional choice for treating osteomyelitis to control bacterial infection.[9] Treating osteomyelitis by oral or intravenous administration of systemic antibiotic therapy, can be effective.[10] However, the effectiveness of some antibiotics as antimicrobials have limitations that include poor penetrability, which prevents the drug from reaching the minimum inhibitory concentration (MIC) level in bone tissue.[11,12] In addition, high doses of antibiotics administered systemically can induce serious side-effects such as ototoxicity and nephrotoxicity. Given these limitations, there is a clear need for the development of delivery carriers for controlled VCM release to improve its antimicrobial activity and reduce side-effects.

Local therapy is rapidly developing as a promising tool for the treatment of several diseases such as tumors and osteomyelitis.[4,13] This approach can promote the availability of high concentrations of drug at the disease site and can reduce side effects. To reduce the reinfection rate of chronic osteomyelitis therapy, the drug delivery material should be biodegradable to eliminate the need to remove the material after treatment.

Several materials, such as Genta-Coll and Palacos, provide local antibiotic delivery for chronic osteomyelitis therapy and are currently used in clinics.[2] In a previous study, our group constructed a solid VCM drug delivery system for osteomyelitis treatment using poly(trimethylene carbonate).[14] Although this kind of local antibiotic delivery system was biodegradable and effective in treating osteomyelitis, its administration was inconvenient and it could not completely fill irregular bone tissue in vivo, which may lead to incomplete antibacterial effects and bone regeneration.

Hydrogels, particularly thermosensitive hydrogels, are considered promising candidates for partial application of local therapy owing to their moldability, biodegradability, and compositional and morphological similarity to tissues.[15,16] The variety of hydrogels with different material that people have worked on with regards to drug delivery for bone tissue engineering, such as polymer material[17] and short peptides.[18,19] Thermosensitive hydrogels, usually in free-flowing sol states with good injectability at a low or room temperature, injected into the target site, the drug-loaded systems can spontaneously turn into semisolid gels, acting as sustained release depots of drugs and fully fill the damaged area.[20] Chitosan (CS) is commonly used as a tissue regeneration material owing to its antibacterial, pain relief, and hemostasis properties.[17,21] CS can be combined with antibiotics to enhance their antibacterial effects and fight bacterial resistance.[2] Many research groups have prepared CS-based hydrogels as tissue scaffolds for the delivery of antibiotics and to promote tissue repair such as cardiac repair and bone regeneration.[22–25] In addition, CS and glycerol phosphate disodium salt (GP) could be prepared as a thermosensitive hydrogel that has a low viscosity at lower critical solution temperature and turns into a gel state at higher critical solution temperature to fill irregular bone sites.[26] Drug release from CS-gels commonly follows physical diffusion in which the drug cumulative release time only reaches 1–5 days.[27,28] However, clinical antibiotic treatment of osteomyelitis is longer than 4 weeks. Therefore, we need to develop a new CS-based hydrogel drug delivery system to extend antibiotic release times.

Nanosystems have been recently developed as alternatives to antibiotics for the treatment of bacterial infections. However, these advanced systems are limited by system administration and subsequent side effects.[29] Nanoparticle (NPs)-hydrogel drug delivery systems have received much attention for reducing the burst release to achieve sustained and continuous release over long periods in vivo.[30,31] CS-based NPs are more commonly used as a drug carrier to treat a number of diseases because of their biocompatibility and low toxicity. In a previous study, we prepared VCM-loaded N-trimethyl chitosan (TMC) NPs from TMC/tripolyphosphate, which demonstrated activity against *Staphylococcus aureus* in vitro.[32] However, the drug loading of the NPs was low, approximately 5.8±0.2%, leading to dissatisfactory dosage in an in vivo study. A novel, high VCM loaded, CS-based NPs design that can attain the

required dosage after embedding in a hydrogel is therefore required for an in vivo study.

We hypothesize that the positive charge of quaternary ammonium chitosan (QAC) and the negative charge of carboxylated chitosan (CC) can drive the electrostatic adsorption-driven assembly of nanoparticles and produce high encapsulation efficiency and drug loading of the water-soluble drug VCM. To prolong its anti-infection activity and promote bone repair, a bioinspired strategy using CS and GP to form a thermosensitive hydrogel (CS-Gel) and incorporate the VCM-NPs into the CS-Gel was used to construct the injectable thermosensitive VCM-NPs /Gel drug delivery system. The mechanism of the thermosensitive nanosystem from sol to gel and its application were presented in Scheme 1. We expected that VCM-NPs would achieve a high VCM loading efficiency and the VCM-NPs/Gel would achieve localized, controlled and sustained release of VCM and uniform filling of bone defects, ultimately realizing anti-infection treatment and bone repair for osteomyelitis.

Materials and Methods

Materials

CS (MW:600 kDa, DD: 85%), QAC (MW: 100 kDa, DD: 90%), and CC (MW: 50 kDa-150kDa based on viscosity; DD: 80%) were purchased from Zhejiang Golden-Shell Pharmaceutical Ltd. (China). VCM was purchased from Dalian Meilun Biotech Co., Ltd. (China). α-Glycerol phosphate disodium salt (α-GP), β-glycerol phosphate disodium salt (β-GP), and fluorescein isothiocyanate (FITC) were purchased from Sigma Aldrich (USA). Phalloidin was purchased from Yeasen Biotech Co., Ltd. (China). *S. aureus* and osteoblasts (OB) were obtained from Zhejiang Academy of Traditional Chinese Medicine and use was approved by the internal institutional review board.

Preparation and Characterization of the VCM-NPs

The NPs were prepared by self-assembly driven by electrostatic adsorption. Briefly, CC and QAC were dissolved

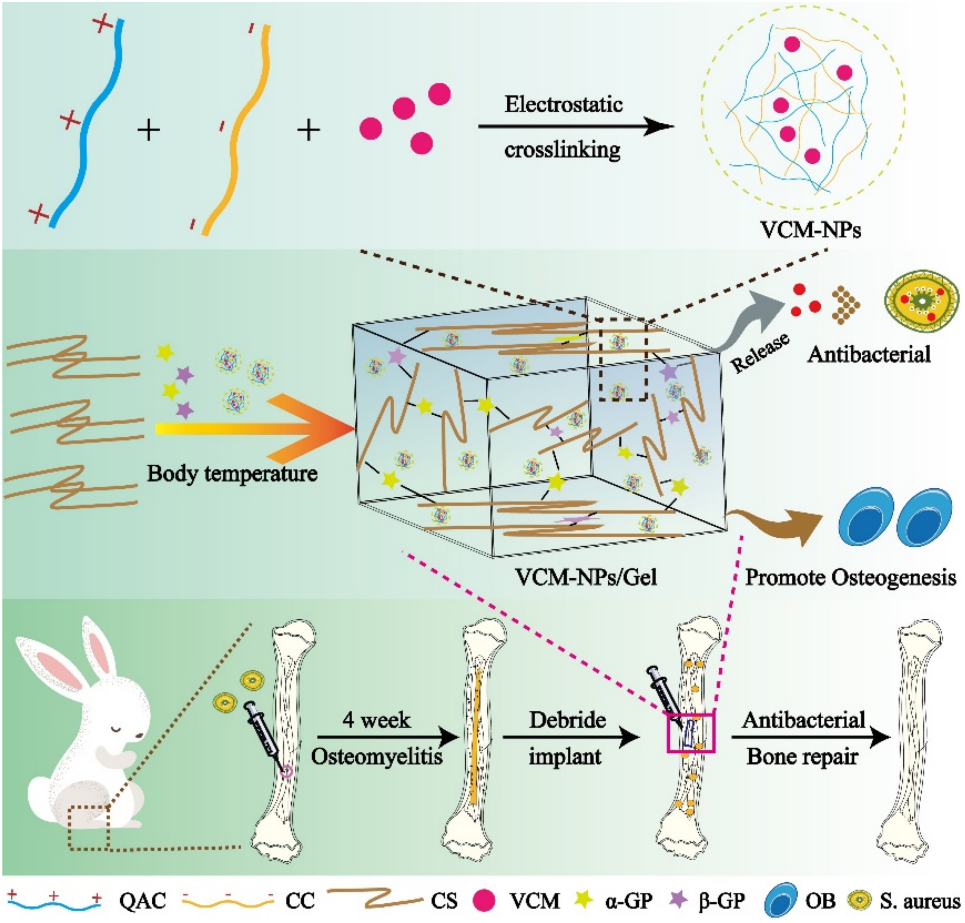

Scheme 1 Schematic diagram of VCM-NPs/Gel for osteomyelitis therapy.

in deionized water at a concentration of 1 mg/mL. The VCM was dissolved in a CC solution with the different weight ratio of VCM/(QAC+CC) (1:1, 1:1.5, 1:2, 1:3), and then CC solution were added dropwise to the QAC solution and mixed immediately under magnetic stirring. The average size and zeta potential of the NPs were measured using a Zeta Sizer Nanoparticle Analyzer (Malvern, UK). The morphology of the NPs was evaluated using transmission electron microscopy (TEM).

The drug loading and encapsulation efficiency of VCM-NPs were determined by ultrafiltration (10 KDa) of the samples at 15,000 rpm for 30 min, followed by high-performance liquid chromatography (HPLC). The absorbance was measured at 230 nm. The drug loading (DL) and encapsulation efficiency (EE) of VCM was calculated by:

$$EE = \left(W_{\text{total drug}} - W_{\text{free drug}}\right)/W_{\text{totaldrug}} \times 100\%$$

$$DL = \left(W_{\text{total drug}} - W_{\text{free drug}}\right)/W_{\text{total materials}} \times 100\%$$

The stability of the VCM-NPs was investigated in phosphate-buffered saline (PBS; 10% fetal bovine serum [FBS], pH 7.4) at room temperature.[33] The size of the NPs was measured at different time points.

Preparation of VCM-NPs/Gel

CS powder was dissolved in 0.1 M acetic acid at room temperature to obtain a homogeneous CS solution with a concentration of 2.5%. Next, α-GP and β-GP (50%, w/v) were dissolved in deionized water and VCM-NPs were incorporated into the GP solution under gentle stirring. Finally, the GP/NP mixture was slowly added dropwise to the CS solution in an ice bath and the mixture was stirred for 15 min. The final solution was incubated at 37°C and the VCM-NPs/Gel hydrogel was formed.

Characterization of the VCM-NPs/Gel

Gelation Time

The gelation time of the hydrogel was measured using the vial inversion method. The hydrogel components at the above concentrations were mixed in a glass sample vial and incubated at 37°C immediately after mixing. The gelation time refers to the time required for no flow to be observed for each formulation.

Scanning Electron Microscopy Analysis (SEM)

The surface morphology of the hydrogel was characterized by SEM. The hydrogels were prepared using the above method and then the hydrogel samples were frozen in liquid nitrogen, and then freeze-dried under vacuum at −70 ºC for 48 h to ensure that water was sublimed sufficiently. The freeze-dried samples were sputter coated with gold.[34] Both the surface and cross-sectional morphologies were examined. SEM images of the hydrogel samples were recorded using a scanning electron microscope (SU8010, Hitachi, Japan) at 5 kV of acceleration voltage, room temperature, and scan speed with TV model (25/30 s/frame).

Swelling and Biodegradation Study

The freeze-dried hydrogels were immersed in PBS (pH 7.4) at 37°C with shaking at 100 rpm. At designated time points, the hydrogels were removed from the PBS, wipe off the liquid from the surface of hydrogel with tissue paper, and weighed.[35]

The biodegradation behavior of the hydrogels was examined in an incubating shaker. Briefly, the freeze-dried hydrogels were immersed in a 0.5 mg/mL lysozyme solution at 37°C with shaking at 100 rpm. At designated time points, the hydrogels were freeze dried and weighed. Changes in the surface morphology were examined by SEM.

The swelling ratio and degradation ratio were calculated using the following equation:

$$\text{Swelling ratio} = (W_e - W_d)/W_d \times 100\%$$

$$\text{Degradation ratio} = (W_d - W_o)/W_d \times 100\%$$

where W_d is the weight of the dry hydrogel at t=0, W_e is the weight of the swollen hydrogel at time t, and W_o is the weight of the dry degraded hydrogel at time t.

Rheological Measurement

Rheological measurements of the hydrogels were performed using a rheometer (Viscotester IQ AIR, HAAKE, Germany) with a 60 mm diameter plate geometry with a gap of 1 mm. The hydrogel solutions were added to the plate of rheometer at 25 °C and then plate with temperature range of 25–45 °C at a heating rate of 0.5 °C/min. The variations of storage (G′) and loss (G″) modulus were measured under constant strain (0.1%) and frequency (1 Hz).

In vitro VCM Release Profile

The release profile for the hydrogel was examined in pH 7.4 PBS media. Briefly, hydrogels were immersed in 4 mL of PBS at 37°C with shaking at 100 rpm. At designated time points, 1 mL of media was removed from each tube and

fresh media was added. The concentration of VCM in the removed aliquots was determined using HPLC equipped with a Diamonsil C_{18} column (250 mm × 4.6 mm, 5 μm) (mobile phase: methanol/potassium dihydrogen phosphate buffer (pH 3.2 and 25 mmol/L) 20:80; flow rate: 0.7 mL/min; detection λ: 230 nm).

The VCM-NPs/Gel solution was placed in a test tube and immersed in a water bath at 37°C to form a gel. Then, 4 mL of PBS buffer was added to the test tube and incubated at 37°C with shaking at 100 rpm. At predefined time intervals, the release media was withdrawn from the test tube and the collected VCM-NPs were detected using a Zeta Sizer Nanoparticle Analyzer.

Cell Proliferation

The VCM-NPs/Gel was tested by a CCK-8 assay. OB cells (obtained from Zhejiang Academy of Traditional Chinese Medicine and use was approved by the Laboratory Animal Ethics Committee, Zhejiang Academy of Traditional Chinese Medicine) were seeded in 96-well plates at 5×10^3/well and cultured overnight. Each group was added to cells at concentrations of 10, 40, and 80 μg/mL VCM. After 24 h and 72 h, 20 μL of CCK-8 was added to each well. After further incubation for 3 h, the absorbance of each well was measured at 450 nm using a microplate reader.

Alkaline Phosphatase (ALP) Expression

OB cells were seeded in 12-well plates at 1×10^5/well and cultured overnight. VCM-NPs and VCM-NPs/Gel were added to produce different concentrations of VCM (10, 40, and 80 μg/mL). After 4 d and 7 d, cells were lysed and the expression of ALP was measured at 520 nm using a microplate reader according to the instructions of the ALP kit (Nanjing Jiancheng Bioengineering Institute). In addition, the total protein concentration was measured using a BCA kit and the ALP activity (per unit/protein) was calculated.

In vitro Antibacterial Activity

Antibacterial Activity Test

S. aureus (ATCC 96) was cultured in Luria-Bertani broth at 37°C overnight at 120 rpm in a shaking incubator until the optical density of the culture medium reached 0.5 at 600 nm. We comprehensively determined the antibacterial activity of the VCM-NPs/Gel using a turbidity test, the diameter of inhibition zone (DIZ) test and the antibacterial effect on the infected OBs.

Turbidity Test

The antibacterial activity of the hydrogels was examined with *S. aureus* using a turbidity test. The hydrogels were extracted with PBS because gels system work slowly and sustain release of VCM. Then, the extract liquid with different drug concentrations was incubated with *S. aureus*. PBS was used as a negative control. The cultures were cultivated overnight in a 37°C incubator shaking at 150 rpm. The optical density of these suspensions was measured at 600 nm on a microplate reader (Multiscan, Thermo, USA).

DIZ Test

To evaluate the antibacterial effects of the hydrogels, the zones of growth inhibition of the test bacteria were measured using an agar disk diffusion assay.[36] Briefly, prepared sterile agar plates and sterile filter disks (round sterile filter paper) were immersed in PBS or extract liquid for 2 h. Four filter disks were then plated on the surface of each agar plate, and the samples were subsequently incubated in a biochemical incubator with an atmosphere of 5% CO_2 at 37°C for 24 h. In addition, for longer cultures against *S. aureus*, the VCM/Gel and VCM-NPs/Gel were evaluated using an Oxford cup test.[34] The hydrogels were removed to fresh inoculated agar plates daily. The DIZ values were measured using a Vernier caliper and the antibacterial effects were positively related to the DIZ values.

Antibacterial Effect on the Infected OBs

OB cells were cultured in RPMI 1640 medium supplemented with 10% FBS at 37°C in a humidified atmosphere containing 5% CO_2 and cells at passage four were used.[14] *S. aureus* and OB cells were cocultured to simulate an in vivo infection. Briefly, *S. aureus* cells were labeled with 100 μg/mL FITC for 4 h, following a previously described protocol with some modification, and the OB cells were seeded into 24 well plates and cultured overnight. Approximately 1×10^6 CFU/mL of *S. aureus* was added to cells to induce intracellular infection and cells were incubated for 2 h in a CO_2-free incubator. VCM, VCM NPs, and VCM-NPs/Gel with VCM concentrations of 10, 40, and 50 μg/mL were then added. The osteoblast nucleus was stained with DAPI and cytoskeletal f-actin with rhodamine phalloidin using a previously described protocol. The number of *S. aureus* cells was determined from four randomly selected images using ImageJ software.

Animal Surgery Protocol

The animal experiments were performed according to protocols reviewed and approved by the Laboratory Animal Welfare Ethics Committee, Zhejiang Academy of Traditional Chinese Medicine. Male New Zealand White rabbits aged 3 months old and weighing 3.0±0.2 kg were housed in individual cages under air-controlled conditions (20°C±1°C and 12 h/12 h light/dark illumination cycles). The model was prepared by creating a 2-mm diameter hole in the tibia of each animal and successively injecting 0.1 mL of the *S. aureus* suspension (Kanin strain, 1×10^8 CFU/mL) into the medullary cavity of the right tibia, as previously reported.[37] The rabbits were divided into the following groups; VCM/Gel, VCM-NPs/Gel, and vancomycin-calcium sulfate (VCS, previously reported preparation[37]). The rabbits in the VCM/Gel and VCM-NPs/Gel groups were subjected to debridement of necrotic tissue by creating two adjacent 4.8-mm diameter holes in the bone, scraping and cleaning the tissue between the two holes, and then implanting the hydrogel (10 mg vancomycin per rabbit). The surgical process of the implant procedure is shown in Figure 1. The rabbits in the model group and control group were housed under the same conditions with no treatment.

After 4 weeks of infection, and 4 and 8 weeks after treatment; inflammatory indices in serum, such as highly sensitive C-reactive protein (CRP) and white blood cell (WBC) count were determined using a blood biochemistry analyzer (HITACHI 7020, Tokyo, Japan). At the end of the experiment, the tibia specimens were examined by micro-computed tomography (micro-CT) (SkyScan 1172 micro-CT scanner; Bruker, Zurich, Switzerland). Scores for the ratio of bone volume/tissue volume (BV/TV), as well as the bone mineral density (BMD), were obtained directly from the 3D model.

The tibia samples were fixed in 10% EDTA, dehydrated, and then embedded. The tissue blocks were sectioned into 5-μm thick specimens and stained with hematoxylin and eosin (H&E) for morphologic analysis. The sections were also pre-treated and stained for IL-6 (1:100; Abcam Ltd., Cambridge, UK).

Statistical Analysis

All data are presented as mean ± standard deviation based on at least three measurements for all results. Statistical analysis was conducted using GraphPad Prism software. The significance was evaluated using a Student's *t*-test and $P<0.05$ was considered statistically significant.

Results and Discussion

Preparation and Characterization of the VCM-NPs

The particle size and zeta potential of the blank NPs gradually decreased with increasing QAC/CC (w/w), which is likely a result of the increasing CC content of the formulation (Figure 2A). The increase in negatively charged CC increase the condensing effect with QAC. The properties of the VCM-NPs changed as the weight ratio of VCM/(QCA+CC) changed, and the optimal formulation of VCM-NPs was VCM/(QAC+CC) 1:1.5 (w/w), which produced VCM-NPs with a particle size of 182.4±8.8 nm, a zeta potential of 20.9±1.5 mV, EE of 60.1±2.1%, and DL of 24.1±0.84% (Table 1). The result showed that the higher VCM content (VCM/(QAC+CC) =1:1) resulted in larger sizes and lower EE of VCM-NPs because the drug loading capacity of the NPs is limited. Additionally, the lower VCM content (VCM/(QAC+CC) =1:2 or 1:3) resulted in lower EE of VCM-NPs. We think that VCM is a water-soluble drug and a low concentration of VCM increases the distance between VCM molecules, which increases the difficulty of encapsulating VCM by NPs in the process of electrostatic adsorption of QAC and CC to package VCM. The EE and DL were greater than a previous report of other VCM-loaded delivery systems, including liposomes (32.65%, 2.18%),[38] niosomes (50.47%, 19.0%),[39] and micelles (35%, 4.5%), respectively.[40] The VCM-NP assembly

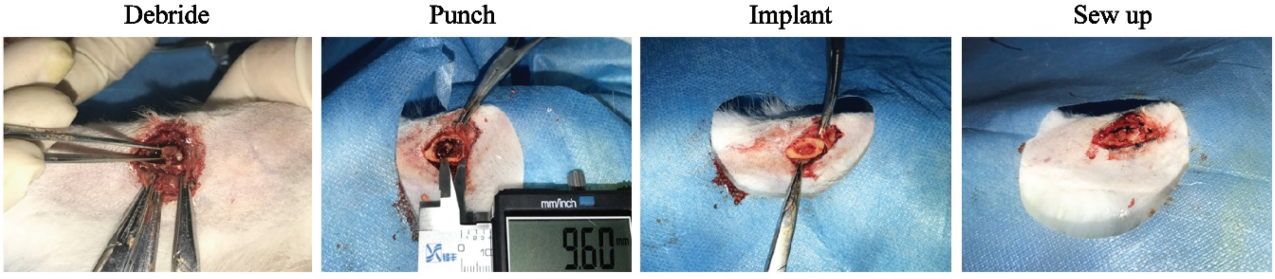

Figure 1 Surgical implantation process, including debriding of necrotic tissue, punching two adjacent 4.8-mm diameter holes, implanting the hydrogels, and sewing up.

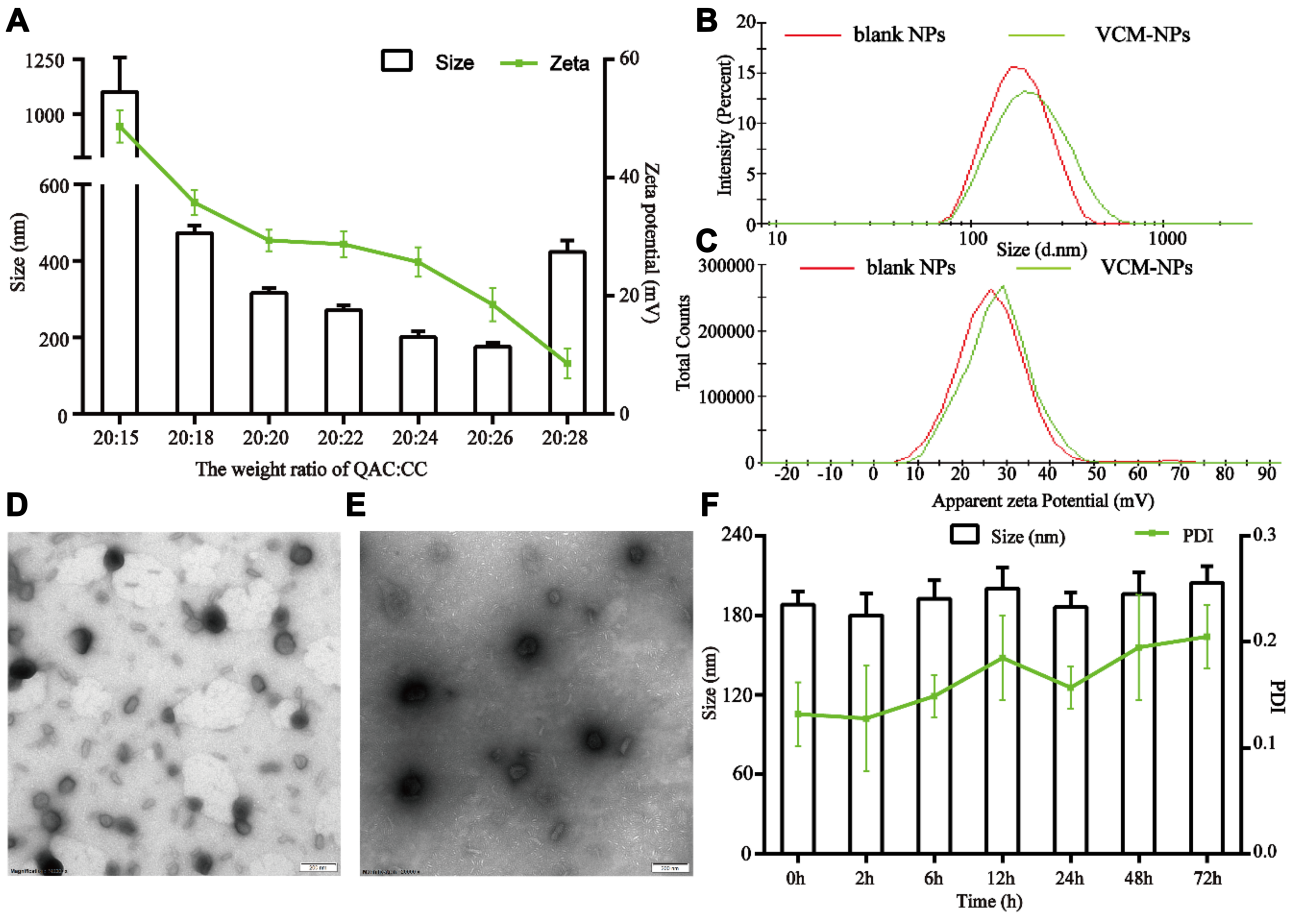

Figure 2 The physical characteristic of VCM-NPs. (**A**) Changes of size distribution and zeta potential of NPs following various weight ratio of QAC/CC; (**B**) size histogram; (**C**) zeta potential; (**D** and **E**) TEM image of blank NPs and VCM-NPs; (**F**) serum stability.

was further optimized by changing the VCM dissolution media (Table 2). The particle size and zeta potential of the VCM-NPs showed a slight increase compared with the blank NPs (Figure 2B and C). The TEM images showed that blank NPs and VCM-NPs were spherical with a uniform size distribution, and the size of the blank NPs and VCM-NPs was approximately 140 nm (Figure 2D and E). The particle sizes and polydispersity indices (PDIs) showed little change for VCM-NPs over 72 h incubated with 20% FBS (Figure 2F), indicating that there was little evidence of nanoparticle aggregation when incubated with serum. However, necrotic bone and irregular bone tissue, which require 4 weeks of antibiotic treatment, are also challenges in osteomyelitis treatment.[10,14] Therefore, it was necessary to further construct a VCM-NP-based local delivery system for sustained release of VCM to optimize the therapeutic approach.

Table 1 The Characteristic of Nanoparticles (n=3)

	Size (nm)	Zeta (mV)	EE (%)	DL (%)
Blank NPs	175.6±10.2	18.5±2.8	ns	ns
VCM-NPs[a]	252.5±8.5	19.0±0.5	40.6±1.5%	20.1±1.2%
VCM-NPs[b]	182.4±8.8	20.9±1.5	60.1±2.1%	24.1±0.84%
VCM-NPs[c]	180.8±7.6	21.7±3.0	45.8±3.5%	26.0±0.73%
VCM-NPs[d]	191.8±6.8	22.2±2.1	44.2±5.8%	13.5±0.97%

Note: [a, b, c, d]Nanoparticles were prepared with different weight ratio of VCM/(QAC+CC) (1:1, 1:1.5, 1:2, 1:3, respectively).

Table 2 The Characteristic of VCM-NPs with VCM Dissolved in Different Media (n=3)

	Size (nm)	Zeta (mV)	EE (%)	DL (%)
VCM-NPs[a]	180.5±6.3	21.8±1.3	30.1±2.5%	12.0±0.99%
VCM-NPs[b]	182.4±8.8	20.9±1.5	60.1±2.1%	24.1±0.84%
VCM-NPs[c]	182.8±5.6	20.0±1.4	35.7±2.6%	14.3±1.04%
VCM-NPs[d]	184.8±4.9	21.4±1.1	50.2±4.8%	20.1±1.93%

Note: [a, b, c, d] VCM-NPs were prepared which the VCM dissolved in QAC, CC, QAC and CC (1:1), QAC and CC (2:1), respectively.

Preparation and Characterization of the VCM-NPs/Gel

Scaffolds are commonly used in tissue engineering of bone for local delivery of antibiotics to improve therapeutic efficacy and reduce systemic toxicity.[41] Therefore, in this study, we developed a novel local delivery system based on VCM-NPs loaded into injectable hydrogels composed of CS and α, β-GP, demonstrating sustained drug release and improved bioactivity. The CS/GP/NPs mixtures were translucent and slightly viscous liquids (sols) at room temperature and had good injectability (Figure S1). Moreover, they solidified into semisolids (gels) at physiological temperature (Figure 3A) because of CS-GP electrostatic attractions between the ammonium and phosphate groups.[42] The formulation of the hydrogel was optimized to reduce the gelation time. As shown in Figure 3B, examination of the gelation times for various ratios of CS/β-GP showed that higher concentrations of β-GP lead to a shorter gelation times. The gelation time can be further reduced by adding α-GP (Figure 3C). This technique is similar to a previous report.[43] The gelation time of the VCM-NPs/Gel was slightly increased with NP loading compared with the VCM/Gel (Figure 3D). VCM-NPs/Gel exhibits desirable gelation behavior for clinical applications because the sol-to-gel transition temperature is between room temperature and physiological temperature.

As shown in Figure 3E–G and Figure S2, below 30°C, the blank gel and NPs/Gel exhibited low values of η, G′, and G″, and G″ greater than G′, implying good flowability. As the temperature increased, a rapid increase of several orders of magnitude in η, G′, and G″ occurred and G′ was greater than G″, indicating the in situ formation of physical hydrogels. Interestingly, after NPs were embedded in the gel, the gelation time and rheological properties of G′ and G″ also showed changes compared with the blank gel. These findings may be the result of the strong intermolecular hydrogen bonding of the NPs and gel or a weaker electrostatic interaction between NPs and the polymer network.[44] All of the results show that the VCM-NPs/Gel is stable and has good mechanical properties.

The results for hydrogel swelling are shown in Figure 3H, indicating the hydrogels with and without NPs displayed high water uptake, and the swelling ratio was ~6 for the blank gel and VCM/Gel. When the NPs were loaded, the water uptake capacities of the NPs/Gel and VCM-NPs/Gel showed no significant change compared with the blank gel, which suggests that all hydrogels have abundant pores to take up large amounts of water.[45] As shown in Figure 3I, the VCM/Gel and VCM-NPs/Gel exhibited excellent degradation in the lysozyme solution and that presence of NPs did not affect the hydrogel degradation. SEM was used to observe structural changes following treatment with enzyme. Following the incubation time, the structure of the gel changed and even the net structure of the gel was no longer detected (Figure 4), which suggests that the VCM-NPs/Gel has good biodegradability.

SEM was used to observe the microstructure of the prepared hydrogel.[46] The microstructure of the VCM-NPs /Gel also has a porous network (Figure 3J) similar to that of VCM/Gel (Figure 3K), which facilitated the sustained drug release, the entry of cells, and the exchange of nutrients. The particle size and morphology of the VCM-NPs were further observed using high-power field SEM (Figure 3L). The particle size of the VCM-NPs observed by SEM was ~200 nm, which is similar to the findings of dynamic light scattering and TEM, suggesting that VCM-NPs remain integrated in the gel structure.

Drug Release

The drug release properties of VCM-NPs, VCM/Gel, and VCM-NPs/Gel were evaluated in PBS. The release of VCM was measured over a period of 25 days. As shown in Figure 5A, VCM was released from VCM/Gel, VCM-NPs, and VCM-NPs/Gel in a controlled manner, with the VCM-NPs/Gel in particular exhibiting well-controlled release over the 25 days. VCM-NPs, VCM/Gel, and VCM-NPs/Gel all displayed a markedly higher drug release in the initial 10 h, showing cumulative VCM release of approximately 56.6%, 48.9%, and 23.5%, respectively. This indicated that the VCM on the hydrogel surface was released as soon as the gel was immersed in the medium. The release of VCM from VCM-NPs/Gel was sustained and a total release of 65% was achieved within 26 days, which meets the clinical demand of drug administration time.[47] Furthermore, the particle sizes in the supernatant of the release medium were 195.7 nm (PDI 0.221) and 204.5 nm (PDI 0.119) on days 1 and 10, respectively (Figure S3). We confirmed that VCM-NPs can release slowly from the gel network and then release VCM, which is similar to results in a previous report.[46,48] Based on the release results and the degradation of the hydrogel, the mechanism of release from VCM-NPs/Gel is thought to be a combination of diffusion and erosion, which sustained the drug release. Therefore, the CS/β-GP/α-GP hydrogel is an ideal drug carrier for controlled drug release, and the hydrogel loaded with VCM-NPs shows significant potential for biomedical fields,

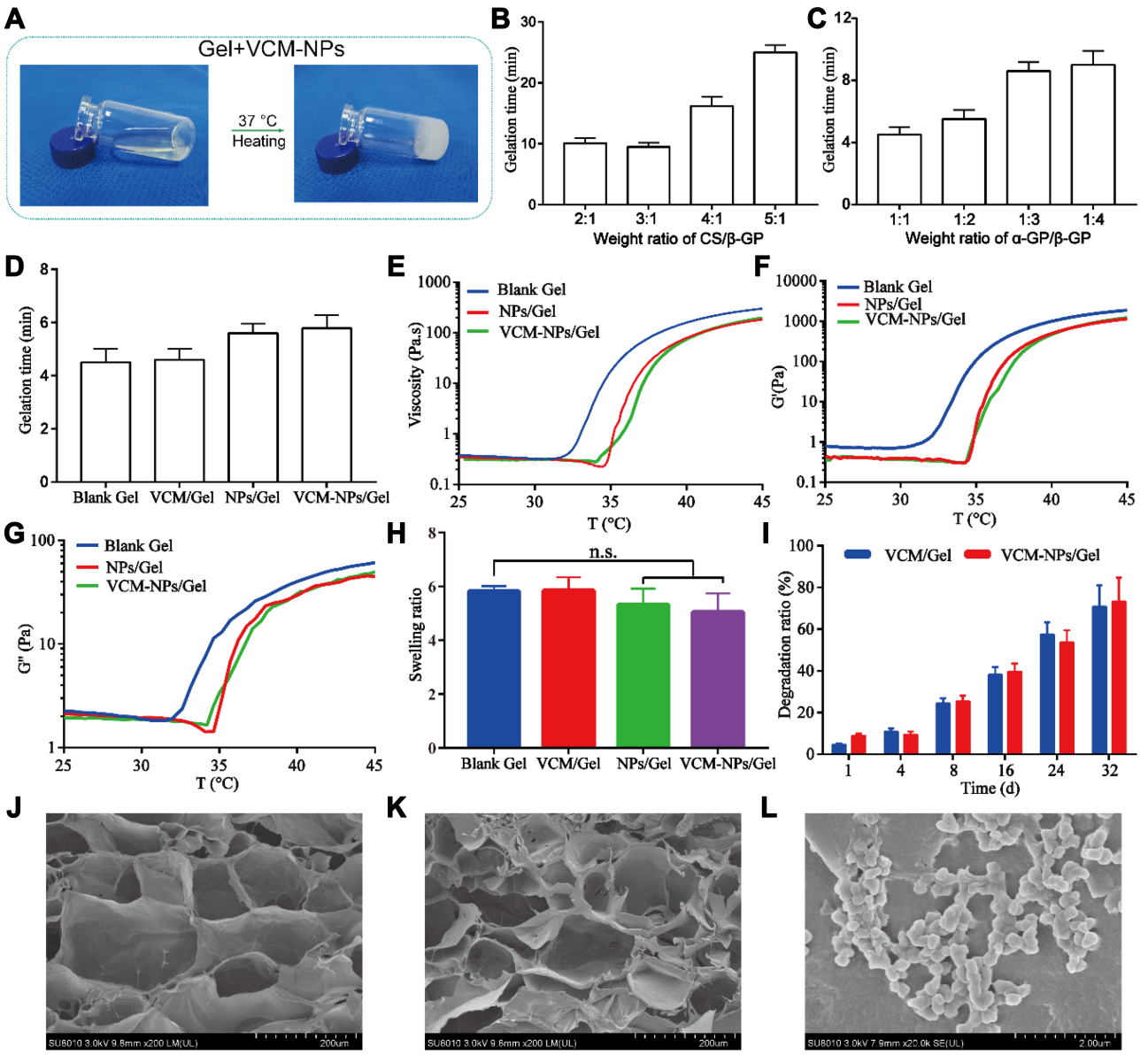

Figure 3 Characterizations of VCM-NPs/Gel. (**A**) Photographs of VCM-NPs/Gel aqueous solutions exhibiting sol and gel states at 20 and 37 °C, respectively. (**B–D**) Gelation time of hydrogel with CS/β-GP, α-GP/β-GP and VCM-NPs, respectively. (**E–G**) Rheological properties exhibiting viscosity (η), storage modulus (G') and loss modulus (G'') of the aqueous solutions of the blank Gel, NPs/Gel and VCM-NPs/Gel as a function of temperature, respectively. (**H**) Equilibrium swelling ratio of hydrogels after swelling for 24 h in PBS (pH 7.4). (**I**) Degradation profiles of the hydrogels in PBS with lysozyme. (**J**) SEM image of VCM/Gel. (**K** and **L**) SEM image and enlarged SEM image of VCM-NPs/Gel.

including as materials for soft tissue defect repair and cell scaffolds.

In vitro Cytotoxicity

Hydrogels are also used as cell scaffolds to accelerate cell proliferation. The primary requirement of scaffolds in tissue engineering is low toxicity. As shown in Figure 5B and C, the VCM and VCM-NPs groups did not show obvious cytotoxicity with different concentrations of VCM (10, 40, and 80 μg/mL) at 24 and 72 h, only VCM-NPs with high VCM concentrations exhibited slight cytotoxicity, which may be caused by the positively-charged NPs. Some studies have suggested that CS/GP hydrogel may inhibit cell proliferation owing to the concentration of GP.[49] The VCM/Gel and VCM-NPs/Gel group did not promote OB cell proliferation with different concentrations of VCM at 24 h. At 72 h, VCM/Gel and VCM-NPs/Gel samples showed a significant increase in OB cell proliferation with dose dependence. The gel may act as a cell scaffold providing a conducive space and environment for growth or CS may promote OB

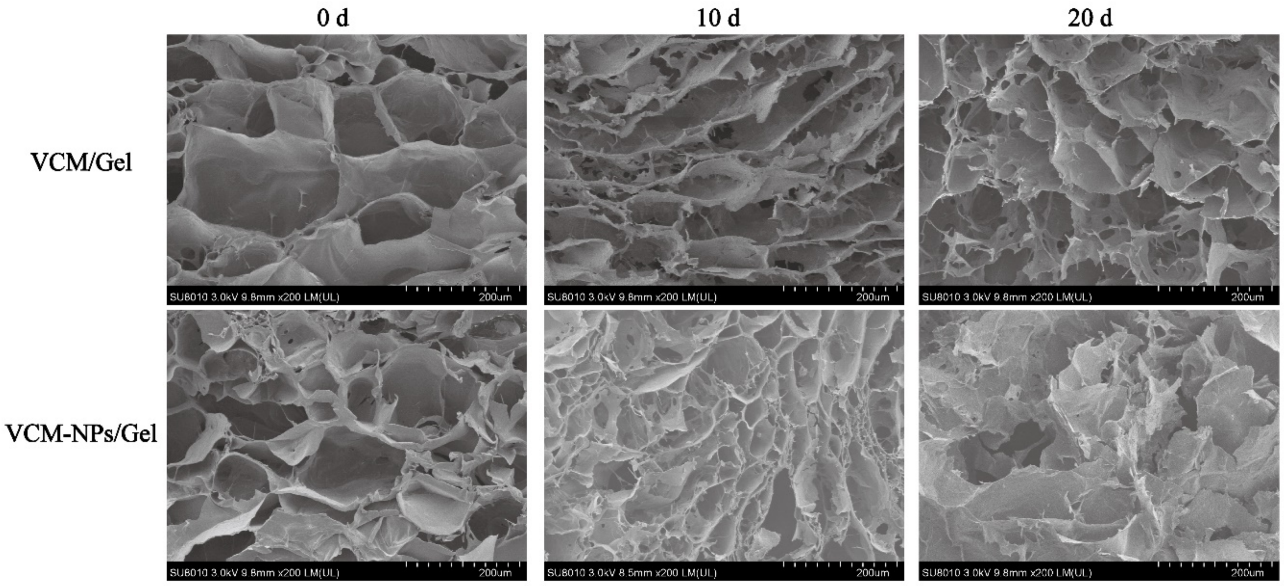

Figure 4 SEM images of the surfaces of VCM/Gel and VCM-NPs/Gel after incubation in PBS 7.4 aqueous medium at 37°C with 0 days, 10 days and 20 days. Note: SEM images of VCM/Gel and VCM-NPs/Gel (0 d) were same as Figure 3 **(J, K)** duo to clear comparative analysis of gel surfaces changes with degradation.

cell proliferation, which is similar to a previous study in which Lu[50] administered intra-articular injections of a CS solution and the cartilage density significantly increased. The function of OBs is also a key factor of bone repair and thus we tested the ALP activity of OB cells. VCM-NPs with different concentrations did not change the ALP activity of the OB cells at 4 d (Figure S4) and 7 d, which is in agreement with the OB cells proliferation results. After treatment with VCM-NPs/Gel, the ALP activity of the OB cells showed a significant increase and the ALP activity was expressed as 179.2, 198.4, and 218.6 king unit/gprot after treatment with 10, 40, and 80 μg/mL VCM concentrations of VCM-NPs/Gel for 7 d, respectively (Figure 5D). The VCM-NPs /Gel was not only cytocompatible but also conducive to OB cell proliferation, making it an ideal scaffold for bone regeneration.

In vitro Antibacterial Activity

Because the occurrence and treatment of osteomyelitis are generally accompanied by a high incidence of bacterial infection, antibacterial treatment is a key element of osteomyelitis therapy.[4] As shown in Figure 6A, VCM, VCM-NPs, and VCM-NPs/Gel exhibited good activity against *S. aureus* in a concentration-dependent manner. Efficacy against *S. aureus* was observed in the following order, VCM-NPs/Gel>VCM-NPs>Free VCM, because aqueous extracts of VCM-NPs/Gel contain VCM and CS, and CS can also damage the cell walls of the bacteria.[51] Figure 6B shows that an inhibition zone was observed for the VCM, VCM-NPs, and VCM-NPs/Gel groups and was dose-dependent in all cases, similar to the findings of the turbidimetric analysis. Interestingly, VCM-NPs showed greater activity against *S. aureus* than VCM, which may be because of the positively charged NPs that were effective in binding to the negatively-charged cell membrane of the bacteria, leading to leakage of the intracellular components and bacterial death.[52] The Oxford cup method of DIZ testing was used to illustrate the sustained release and prolonged antibacterial activity of the gel system (Figure 6C and D). Before the hydrogels were loaded with VCM or VCM-NPs, they did not exhibit antibacterial effects against *S. aureus* (Figure 6C a–b and Figure S5). The inhibition zone of the VCM/Gel showed a sudden and significant decrease at day 5 and showed no effect against *S. aureus* at day 10 as a result of rapid VCM release (Figure 5A). In comparison, the VCM-NPs/Gel showed prolonged activity against *S. aureus* of more than 20 days, which suggested that the VCM-NPs/Gel had more sustained and stable antibacterial properties. Figure 6E shows the bacterial colonies cultured with VCM, VCM-NPs, VCM/Gel, and VCM-NPs/Gel at days 1 and 15. At day 1, there were few visible bacterial colonies for all groups, with their numbers of bacterial colonies in the following order: VCM< VCM/Gel< VCM-NPs/Gel< VCM-NPs. At day 15, the number of bacterial colonies order was substantially different at VCM-NPs/Gel< VCM/

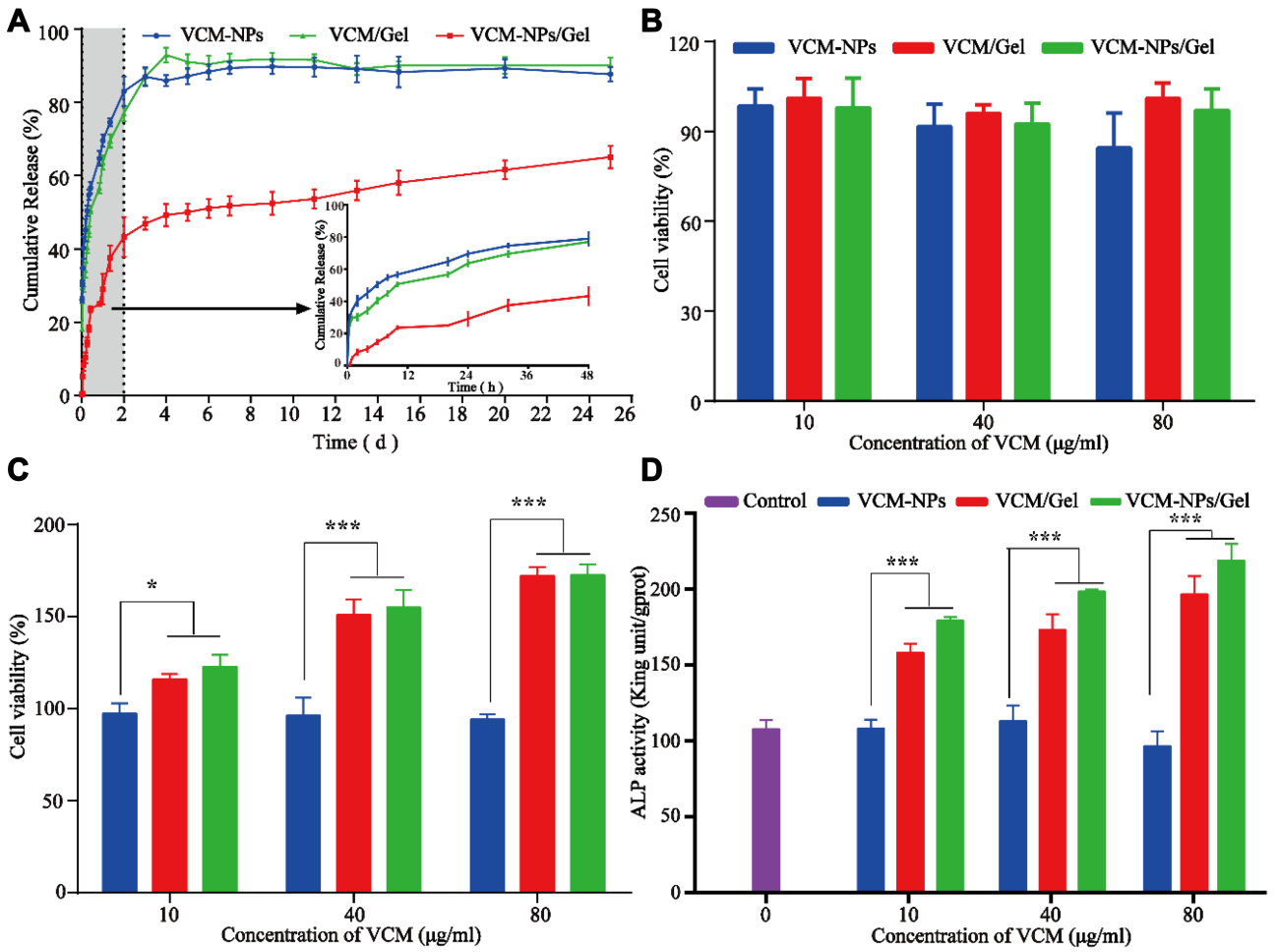

Figure 5 VCM release and OB cells biocompatibility evaluation in vitro. (**A**) In vitro release profiles of VCM-NPs, VCM/Gel and VCM-NPs/Gel. (**B** and **C**) CCK-8 results of OB cells treated with VCM-NPs, VCM/Gel and VCM-NPs/Gel with different concentration at 24 h and 72 h, respectively. (**D**) ALP activity of OB cells treated with VCM-NPs, VCM/Gel and VCM-NPs/Gel with different concentration at 7 days. *P< 0.05; ***P< 0.001.

Gel< VCM< VCM-NPs< Control. This result also suggests sustained release of VCM and prolonged antibacterial activity in the VCM-NPs/Gel.

We investigated the ability of the antibiotics to eradicate *S. aureus* from infected OBs while preserving their osteogenic potency.[14] As shown in Figure 7, following 2 h of coculture, labeled bacteria became visible inside the infected OBs, while after 24 h of incubation of infected OB with VCM, VCM-NPs, and VCM-NPs/Gel, the number of bacteria visible both inside and outside the cells was significantly reduced compared with the model group. Compared with the free VCM-treated samples, VCM-NPs samples showed a decrease in the *S. aureus* inside the OBs because the OBs uptake of NPs was higher than that of the free drug. In addition, when the VCM-NPs/Gel concentration was increased, the bacteria visible both inside and outside the cells decreased.

In vivo Anti-Infection Capability

Animal models are necessary to demonstrate osteomyelitis therapy in vivo.[53] Rabbit is one of the most commonly used species for osteomyelitis-related studies as they have sufficiently large bones to tolerate surgical trauma and a similar temperature sensitivity to that of humans, which enhances the applicability of the evaluation. In our study, we chose rabbit as a model animal and used 1×10^7 CFU to stimulate osteomyelitis in the model, as in our previous report.[14,37] Four weeks after infection with *S. aureus*, white and yellow pus was discharged from the rabbit leg wounds, similar to the representative symptom of chronic osteomyelitis observed in clinics. CRP and WBC are important indicators of bacterial infection and provide a basic method for clinical diagnosis. Compared with the control group, the levels of CRP and WBC were higher in the model group at the end of the 4th week following infection with *S. aureus* (Figure 8A and B).

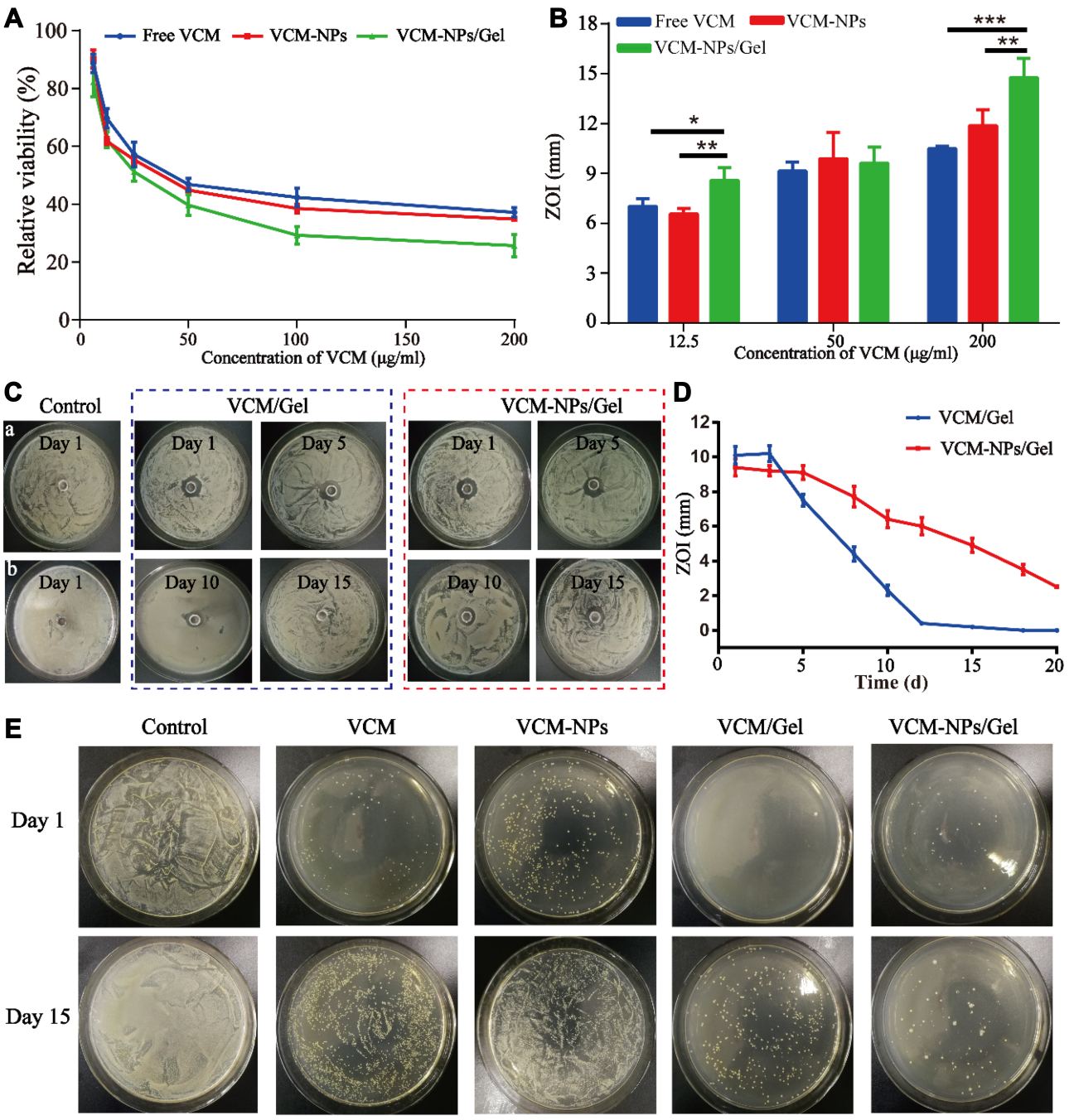

Figure 6 Anti-bacterial of hydrogel. The VCM, VCM-NPs and extract liquid of VCM-NPs/Gel against *S. aureus* by turbidimetric method (**A**) and inhibition zone method (**B**). (**C**) Optical images of antibacterial activity of VCM/Gel and VCM-NPs/Gel against *S. aureus* for different time points. Control groups without VCM: Gel (a) and blank-NPs /Gel (b). (**D**) The quantify of inhibition zone of VCM/Gel and VCM-NPs/Gel against *S. aureus*. (**E**) Bacterial colonies formed using an agar diffusion assay after contacting with different group at 1 day and 15 day. **P*< 0.05; ***P*< 0.01, ****P*< 0.001.

However, 4 and 8 weeks after treatment with VCM/Gel, VCM-NPs/Gel, and VCS, both antibiotic delivery systems significantly reduced the CRP and WBC levels compared with the model group. At the end of the 4th week post-treatment, the level of WBC in the VCM-NPs/Gel group was less than that for the VCM/Gel and VCS groups. The level of CRP in the VCM-NPs/Gel group decreased significantly compared with the VCM/Gel group, however there was no significant difference compared with the VCS group.

Radiographic Data

In a typical bone regeneration process, scaffolds placed in bone defect sites can lead to rapid initiation of efficient cell

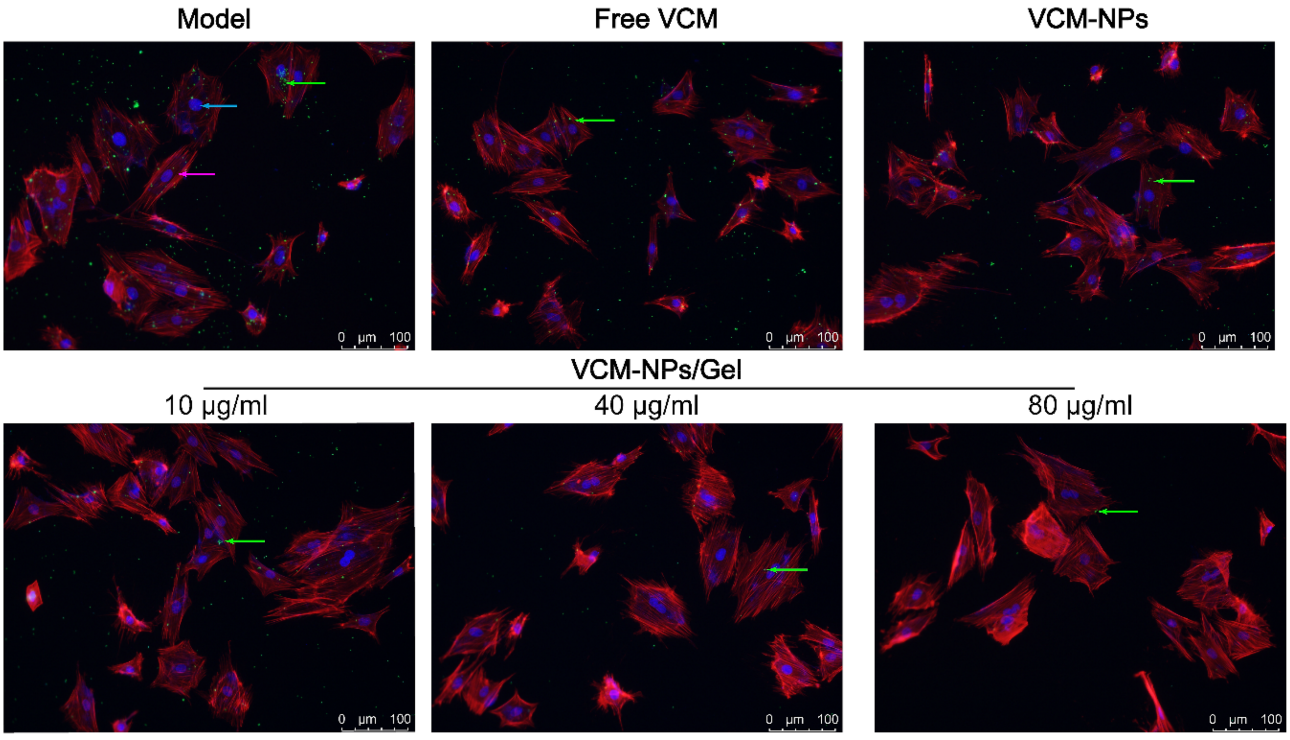

Figure 7 Fluorescence images of fluorescently stained osteoblastic cell nuclei (blue arrow) and cytoskeletal F-actin (red arrow), invaded by *Staphylococcus aureus* (green arrow). Free VCM and VCM-NPs with VCM concentration of 40 μg/mL.

recruitment, adhesion, proliferation, and osteodifferentiation, which are important for bone regeneration and bone remodeling.[54,55] Eight weeks after treatment, the tibia plateau of the VCM-NPs/Gel group appeared flatter than that of the VCM/Gel group. The images of the 3D reconstruction in Figure 8C indicate a progressive increase in bone volume at the end of the 8th week post-treatment with VCM/Gel, VCM-NPs/Gel, and VCS, while it tended toward bone loss in the model groups. In addition, the tibia plateau in the VCS group seemed flatter than that of the VCM/Gel and VCM-NPs/Gel groups. The micro-CT indices (Figure 8D and E) showed that the BV/TV and BMD decreased further and were significantly lower in the model group than in the VCM/Gel, VCM-NPs/Gel, and VCS groups. In addition, the BV/TV and BMD were markedly higher in the VCM-NPs/Gel group than in the VCM/Gel group. These results suggest that the VCM-NPs/Gel promotes bone healing.

Histopathological Analysis

The untreated animals of the model groups showed severe osteomyelitis, exhibited polymorphonuclear leukocyte infiltration, fibrotic tissue with a high number of proliferative lymphocytes, and some plasma cells.[47] The animals treated with VCM/Gel, VCM-NPs/Gel, and VCS showed fewer inflammatory cells than the model group (Figure 9A). After modeling, infection with *S. aureus* caused a decrease in the number of bone trabeculae; however the VCM/Gel, VCM-NPs/Gel, and VCS groups showed less pronounced decreases than the model group (Figure 9C and D). The number of OBs per trabecular bone area (NOb/TAr) and the number of OBs per bone perimeter (NOb/Bpm) were reduced in the control group, as the OBs were in a static state. A pronounced decrease in NOb/TAr and NOb/Bpm was induced by *S. aureus*; however this decrease was mitigated by the VCM/Gel, VCM-NPs/Gel, and VCS treatments, although NOb/Bpm in the VCM-NPs /Gel group showed no significant difference in the VCS group.

To more sensitively detect infection and inflammation, IL-6 was combined with CRP and WBC. IL-6 is a multifunction cytokine related to cancer, infection, and obesity. As shown in Figure 9B and E, significantly decreased rates of integrated optical density/area (IOD/area) for IL-6 were observed for the VCM/Gel, VCM-NPs/Gel, and VCS groups compared with the model group and this was more pronounced in the VCM-NPs/Gel and VCS groups. Therefore, the VCM-NPs/Gel showed the ability to enhance osteogenesis and also control infection both in vitro and in vivo.

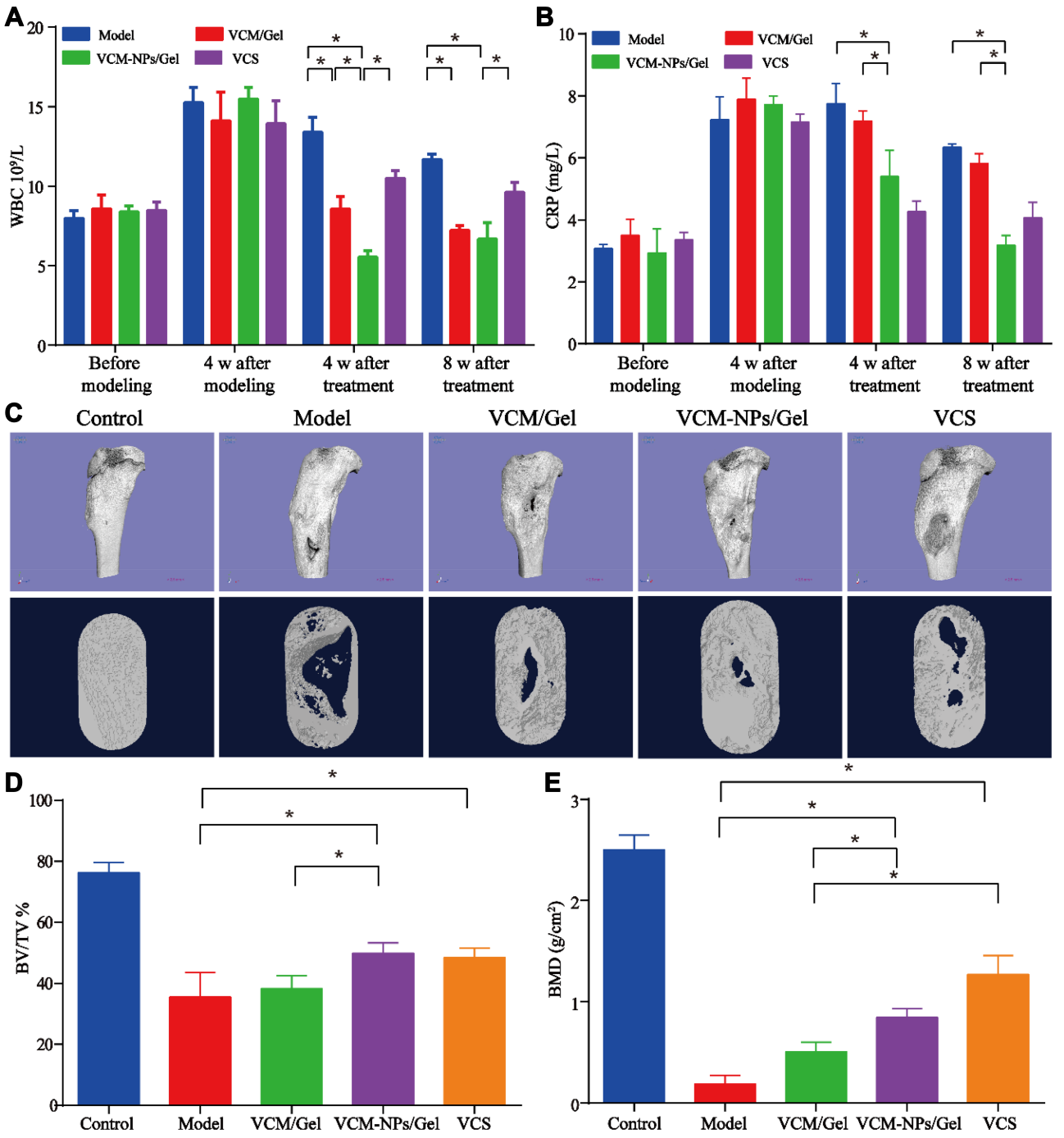

Figure 8 In vivo anti-infection and bone repair capability in a chronic osteomyelitis rabbit model after treat with hydrogel. (**A** and **B**) The results of CRP and WBC in the rabbit serum at the before modeling, fourth week after modeling and the fourth week and eighth week after treatment. (**C**) Micro-CT morphometry of bone defect of the tibia in chronic osteomyelitis model rabbits after treat VCM/Gel, VCM-NPs/Gel and VCS. (**D** and **E**) Micro-CT-quantified histograms of BV/TV and BMD from five rabbits per group. *P< 0.05.

Conclusion

In this study, we demonstrated a simple and effective local drug delivery system based on VCM-NPs, which have high EE and DL of VCM, loaded into a CS/GP thermosensitive hydrogel for treatment of *S. aureus*-induced chronic osteomyelitis. Not only did the VCM-NPs/Gel system sustain VCM release over 26 day and offer excellent injectability and thermosensitivity, the system also promoted OB proliferation and prolonged activity against *S. aureus*. Furthermore, the in vivo study showed that the implantation of VCM-NPs/Gel in a rabbit model resulted in anti-infection activity and promoted OB proliferation at

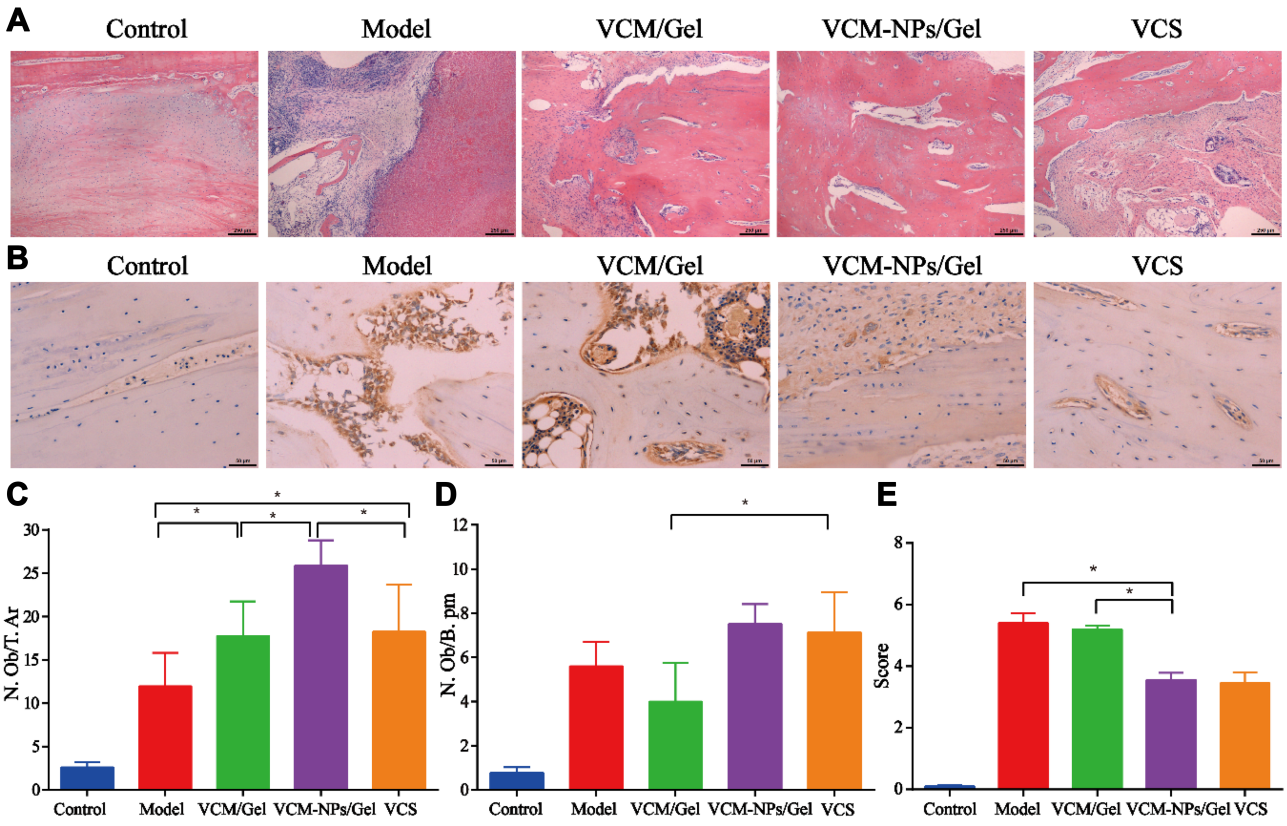

Figure 9 Histological and immunohistochemical examination of rat bones for animals. (**A**) Typical histopathology of the rabbit tibia. (**B**) IL-6 immunohistochemical of the rabbit tibia. (**C** and **D**) The columns represent the scores of osteoblast number/trabecular bone area (NOb/TAr); osteoblast number/bone perimeter (NOb/Bpm). (**E**) The columns represent the IOD/area rate of immunohistochemical staining for IL-6. *P< 0.05.

the bone defect site. We believe that this multi-function drug delivery system could be a promising strategy for promoting bone regeneration and preventing or treating infection, which may open new avenues for the healing of osteomyelitis and bone defects/fractures.

Funding

This work was supported by the National Natural Science Foundation of China (No. 81773673 and 81803808), Zhejiang Province Public Welfare Technology Application Research Project of China (No. LGF19H300005 and LGF19H300007), Natural Science Foundation of Ningbo (No. 2018A610263), Key Laboratory of Ningbo, China (No. 2016A22002), Zhejiang University Student Science and Technology Innovation Activity Plan (No. 2017R435003), Foundation of Zhejiang educational committee (No. Y201738467) and Scientific Research Project of Zhejiang Pharmaceutical College (No. ZPCSR2017004). We thank Sarah Dodds, PhD, and Ashleigh Cooper, PhD, from Liwen Bianji, Edanz Editing China, for editing the English text of a draft of this manuscript.

Disclosure

The authors declare no conflicts of interest for this work.

References

1. Lew DP, Waldvogel FA. Osteomyelitis. *Lancet*. 1997;336 (14):369–379. doi:10.1056/NEJM199704033361406
2. Kavanagh N, Ryan EJ, Widaa A, et al. Staphylococcal osteomyelitis: disease progression, treatment challenges, and future directions. *Clin Microbiol Rev*. 2018;31(2):e00084–00017. doi:10.1128/CMR.00084-17
3. Walter G, Kemmerer M, Kappler C, Hoffmann R. Treatment algorithms for chronic osteomyelitis. *Dtsch Arztebl Int*. 2012;109 (14):257–264. doi:10.3238/arztebl.2012.0257
4. Nandi SK, Bandyopadhyay S, Das P, et al. Understanding osteomyelitis and its treatment through local drug delivery system. *Biotechnol Adv*. 2016;34(8):1305. doi:10.1016/j.biotechadv.2016.09.005
5. Dudareva M, Hotchen AJ, Ferguson J, et al. The microbiology of chronic osteomyelitis: changes over ten years. *J Infect*. 2019;79 (3):189–198. doi:10.1016/j.jinf.2019.07.006
6. Abe K, Cox A, Takamatsu N, et al. Gain-of-function mutations in a member of the Src family kinases cause autoinflammatory bone disease in mice and humans. *Proc Natl Acad Sci*. 2019;116 (24):11872–11877. doi:10.1073/pnas.1819825116
7. Wei J, Wang Y, Jiang J, et al. Development of an antibacterial bone graft by immobilization of levofloxacin hydrochloride-loaded mesoporous silica microspheres on a porous scaffold surface. *J Biomed Nanotechnol*. 2019;15(5):1097–1105. doi:10.1166/jbn.2019.2743

8. Fathi M, Akbari B, Taheriazam A. Antibiotics drug release controlling and osteoblast adhesion from titania nanotubes arrays using silk fibroin coating. *Mat Sci Eng C-Mater*. 2019;103:109743. doi:10.1016/j.msec.2019.109743
9. Lora-Tamayo J, Murillo O. Shorter treatments for vertebral osteomyelitis. *Lancet*. 2015;385(9971):836–837. doi:10.1016/S0140-6736(14)61936-X
10. Li H, Rombach I, Zambellas R, et al. Oral versus intravenous antibiotics for bone and joint infection. *N Engl J Med*. 2019;380(5):425–436. doi:10.1056/NEJMoa1710926
11. Jelinkova P, Mazumdar A, Sur VP, et al. Nanoparticle-drug conjugates treating bacterial infections. *J Control Release*. 2019;307:166–185. doi:10.1016/j.jconrel.2019.06.013
12. Munita JM, Arias CA. Mechanisms of antibiotic resistance. *Microbiol Spectr*. 2016;4(2). doi:10.1128/microbiolspec.VMBF-0016-2015
13. Cheng CA, Deng T, Lin FC, Cai Y, Zink JI. Supramolecular nanomachines as stimuli-responsive gatekeepers on mesoporous silica nanoparticles for antibiotic and cancer drug delivery. *Theranostics*. 2019;9(11):3341–3364. doi:10.7150/thno.34576
14. Zhang Y, Liang R, Xu J, et al. Efficient induction of antimicrobial activity with vancomycin nanoparticle-loaded poly(trimethylene carbonate) localized drug delivery system. *Int J Nanomed*. 2017;12:1201–1214. doi:10.2147/IJN.S127715
15. Cheng J, Amin D, Latona J, Heber-Katz E, Messersmith PB. Supramolecular polymer hydrogels for drug-induced tissue regeneration. *ACS Nano*. 2019;13(5):5493–5501. doi:10.1021/acsnano.9b00281
16. Sahoo JK, VandenBerg MA, Webber MJ. Injectable network biomaterials via molecular or colloidal self-assembly. *Adv Drug Deliv Rev*. 2018;127:185–207. doi:10.1016/j.addr.2017.11.005
17. Annamalai RT, Hong X, Schott NG, Tiruchinapally G, Levi B, Stegemann JP. Injectable osteogenic microtissues containing mesenchymal stromal cells conformally fill and repair critical-size defects. *Biomaterials*. 2019;208:32–44. doi:10.1016/j.biomaterials.2019.04.001
18. Chan K, Zhuo S, Ni M. Natural and synthetic peptide-based biomaterials for bone tissue engineering. *OA Tissue Eng*. 2013;1(1):6. doi:10.13172/2052-9643-1-1-787
19. Chan K, Lee W, Zhuo S, Ni M. Harnessing supramolecular peptide nanotechnology in biomedical applications. *Int J Nanomed*. 2017;12:1171–1182. doi:10.2147/IJN.S126154
20. Shen W, Chen X, Luan J, Wang D, Yu L, Ding J. Sustained codelivery of cisplatin and paclitaxel via an injectable prodrug hydrogel for ovarian cancer treatment. *ACS Appl Mater Interfaces*. 2017;9(46):40031–40046. doi:10.1021/acsami.7b11998
21. Delezuk JA, Ramírez-Herrera DE, Esteban-fernández de Ávila B, Wang J. Chitosan-based water-propelled micromotors with strong antibacterial activity. *Nanoscale*. 2017;9(6):2195–2200. doi:10.1039/c6nr09799e
22. Tripodo G, Trapani A, Rosato A, et al. Hydrogels for biomedical applications from glycol chitosan and PEG diglycidyl ether exhibit pro-angiogenic and antibacterial activity. *Carbohydr Polym*. 2018;198:124–130. doi:10.1016/j.carbpol.2018.06.061
23. Young S, Sherman S, Cooper T, et al. Mechanically resilient injectable scaffolds for intramuscular stem cell delivery and cytokine release. *Biomaterials*. 2018;159:146–160. doi:10.1016/j.biomaterials.2018.01.008
24. Mahanta AK, Senapati S, Paliwal P, Krishnamurthy S, Hemalatha S, Maiti P. Nanoparticle-induced controlled drug delivery using chitosan-based hydrogel and scaffold: application to bone regeneration. *Mol Pharm*. 2019;16(1):327–338. doi:10.1021/acs.molpharmaceut.8b00995
25. Shu Y, Hao T, Yao F, et al. Correction to RoY peptide modified chitosan-based hydrogel to improve angiogenesis and cardiac repair under hypoxia. *ACS Appl Mater Interfaces*. 2018;10(42):36583. doi:10.1021/acsami.8b14595
26. Wu J, Zheng K, Huang X, et al. Thermally triggered injectable chitosan/silk fibroin/bioactive glass nanoparticle hydrogels for in-situ bone formation in rat calvarial bone defects. *Acta Biomater*. 2019;91:60–71. doi:10.1016/j.actbio.2019.04.023
27. Ruan H, Yu Y, Liu Y, Ding X, Guo X, Jiang Q. Preparation and characteristics of thermoresponsive gel of minocycline hydrochloride and evaluation of its effect on experimental periodontitis models. *Drug Deliv*. 2016;23(2):525–531. doi:10.3109/10717544.2014.929195
28. Haider M, Hassan M, Ahmed I, Shamma R. Thermogelling platform for baicalin delivery for versatile biomedical applications. *Mol Pharm*. 2018;15(8):3478–3488. doi:10.1021/acs.molpharmaceut.8b00480
29. Qi G, Zhang D, Liu F, Qiao Z, Wang H. An "on-site transformation" strategy for treatment of bacterial infection. *Adv Mater*. 2017;29(36):1703461. doi:10.1002/adma.201703461
30. Zheng L, Li C, Huang X, et al. Thermosensitive hydrogels for sustained-release of sorafenib and selenium nanoparticles for localized synergistic chemoradiotherapy. *Biomaterials*. 2019;216:119220. doi:10.1016/j.biomaterials.2019.05.031
31. Ma Y, Cortez-Jugo C, Li J, et al. Engineering biocoatings to prolong drug release from supraparticles. *Biomacromolecules*. 2019;20(9):3425–3434. doi:10.1021/acs.biomac.9b00710
32. Xu J, Xu B, Shou D, Xia X, Hu Y. Preparation and evaluation of vancomycin-loaded n-trimethyl chitosan nanoparticles. *Polymers*. 2015;7(9):1850–1870. doi:10.3390/polym7091488
33. Hosseini ES, Nikkhah M, Hosseinkhani S. Cholesterol-rich lipid-mediated nanoparticles boost of transfection efficiency, utilized for gene editing by CRISPR-Cas9. *Int J Nanomed*. 2019;14:4353–4366. doi:10.2147/IJN.S199104
34. Zhu J, Li F, Wang X, Yu J, Wu D. Hyaluronic acid and polyethylene glycol hybrid hydrogel encapsulating nanogel with hemostasis and sustainable antibacterial property for wound healing. *ACS Appl Mater Interfaces*. 2018;10(16):13304–13316. doi:10.1021/acsami.7b18927
35. Yuan X, Amarnath Praphakar R, Munusamy M, Alarfaj A, Suresh Kumar S, Rajan M. Mucoadhesive guargum hydrogel inter-connected chitosan-g-polycaprolactone micelles for rifampicin delivery. *Carbohydr Polym*. 2019;206:1–10. doi:10.1016/j.carbpol.2018.10.098
36. Bavya MC, Vimal Rohan K, Gaurav GB, Srivasatava R. Synergistic treatment strategies to combat resistant bacterial infections using schiff base modified nanoparticulate - hydrogel system. *Mater Sci Eng C Mater Biol Appl*. 2019;95:226–235. doi:10.1016/j.msec.2018.10.080
37. Zhang Y, Shen L, Mao Z, et al. Icariin enhances bone repair in rabbits with bone infection during post-infection treatment and prevents inhibition of osteoblasts by vancomycin. *Front Pharmacol*. 2017;8:784. doi:10.3389/fphar.2017.00784
38. Yang Z, Liu J, Gao J, Chen S, Huang G. Chitosan coated vancomycin hydrochloride liposomes: characterizations and evaluation. *Int J Pharm*. 2015;495(1):508–515. doi:10.1016/j.ijpharm.2015.08.085
39. Dwivedi A, Mazumder A, Nasongkla N. Layer-by-layer nanocoating of antibacterial niosome on orthopedic implant. *Int J Pharm*. 2018;547(1–2):235–243. doi:10.1016/j.ijpharm.2018.05.075
40. Chen M, Xie S, Wei J, Song X, Ding Z, Li X. Antibacterial micelles with vancomycin-mediated targeting and pH/lipase-triggered release of antibiotics. *ACS Appl Mater Interfaces*. 2018;10(43):36814–36823. doi:10.1021/acsami.8b16092
41. Johnson C, García A. Scaffold-based anti-infection strategies in bone repair. *Ann Biomed Eng*. 2015;43(3):515–528. doi:10.1007/s10439-014-1205-3
42. Wu G, Yuan Y, He J, Li Y, Dai X, Zhao B. Stable thermosensitive in situ gel-forming systems based on the lyophilizate of chitosan/α,β-glycerophosphate salts. *Int J Pharm*. 2016;511(1):560–569. doi:10.1016/j.ijpharm.2016.07.050
43. Zhou HY, Jiang LJ, Cao PP, Li JB, Chen XG. Glycerophosphate-based chitosan thermosensitive hydrogels and their biomedical applications. *Carbohydr Polym*. 2015;117:524–536. doi:10.1016/j.carbpol.2014.09.094

44. Kuang L, Ma X, Ma Y, et al. Self-assembled injectable nanocomposite hydrogels coordinated by in situ generated cap nanoparticles for bone regeneration. *ACS Appl Mater Interfaces*. 2019;11(19):17234–17246. doi:10.1021/acsami.9b03173
45. Qu J, Zhao X, Liang Y, Zhang T, Ma PX, Guo B. Antibacterial adhesive injectable hydrogels with rapid self-healing, extensibility and compressibility as wound dressing for joints skin wound healing. *Biomaterials*. 2018;183:185–199. doi:10.1016/j.biomaterials.2018.08.044
46. Liu H, Shi X, Wu D, et al. Injectable, biodegradable, thermosensitive nanoparticles-aggregated hydrogel with tumor-specific targeting, penetration, and release for efficient postsurgical prevention of tumor recurrence. *ACS Appl Mater Interfaces*. 2019;11(22):19700–19711. doi:10.1021/acsami.9b01987
47. Hassani Besheli N, Mottaghitalab F, Eslami M, et al. Sustainable release of vancomycin from silk fibroin nanoparticles for treating severe bone infection in rat tibia osteomyelitis model. *ACS Appl Mater Interfaces*. 2017;9(6):5128–5138. doi:10.1021/acsami.6b14912
48. Majumder P, Baxa U, Walsh STR, Schneider JP. Design of a multicompartment hydrogel that facilitates time-resolved delivery of combination therapy and synergized killing of glioblastoma. *Angew Chem Int Ed Engl*. 2018;57(46):15040–15044. doi:10.1002/anie.201806483
49. Dang Q, Liu K, Zhang Z, et al. Fabrication and evaluation of thermosensitive chitosan/collagen/α, β-glycerophosphate hydrogels for tissue regeneration. *Carbohydr Polym*. 2017;167:145–157. doi:10.1016/j.carbpol.2017.03.053
50. Lu J, Prudhommeaux F, Meunier A, Sedel L, Guillemin G. Effects of chitosan on rat knee cartilages. *Biomaterials*. 1999;20(20):1937–1944. doi:10.1016/s0142-9612(99)00097-6
51. Leonhardt E, Kang N, Hamad M, Wooley K, Elsabahy M. Absorbable hemostatic hydrogels comprising composites of sacrificial templates and honeycomb-like nanofibrous mats of chitosan. *Nat Commun*. 2019;10(1):2307. doi:10.1038/s41467-019-10290-1
52. Li S, Cui S, Yin D, et al. Dual antibacterial activities of a chitosan-modified upconversion photodynamic therapy system against drug-resistant bacteria in deep tissue. *Nanoscale*. 2017;9(11):3912–3924. doi:10.1039/c6nr07188k
53. Lindsey B, Clovis N, Smith E, Salihu S, Hubbard D. An animal model for open femur fracture and osteomyelitis: part I. *J Orthop Res*. 2010;28(1):38–42. doi:10.1002/jor.20960
54. Bunpetch V, Zhang X, Li T, et al. Silicate-based bioceramic scaffolds for dual-lineage regeneration of osteochondral defect. *Biomaterials*. 2019;192:323–333. doi:10.1016/j.biomaterials.2018.11.025
55. Niu H, Ma Y, Wu G, et al. Multicellularity-interweaved bone regeneration of BMP-2-loaded scaffold with orchestrated kinetics of resorption and osteogenesis. *Biomaterials*. 2019;216:119216. doi:10.1016/j.biomaterials.2019.05.027